RSC Advances

PAPER

View Article Online
View Journal | View Issue

Cite this: *RSC Adv.*, 2020, **10**, 38344

Improving the all-polymer solar cell performance by adding a narrow bandgap polymer as the second donor†

Kai Wang,[a] Sheng Dong,*[b] Xudong Chen,[c] Ping Zhou,[c] Kai Zhang,[b] Jun Huang*[a] and Ming Wang*[a]

Received 15th July 2020
Accepted 23rd September 2020

DOI: 10.1039/d0ra06143c

rsc.li/rsc-advances

Ternary all-polymer solar cells are fabricated using an N2200 acceptor and two donor polymers (PF2 and PM2) with complementary absorption. The major donor PF2 is a relatively wide bandgap polymer that contributes the most photon absorption in the UV-vis region while the second donor PM2 improves the light harvesting due to its strong absorption in the near-IR region. By carefully tuning the ratio of two donor polymers, the best ratio of 9 : 1 : 5 (PF2 : PM2 : N2200) is achieved and shows a PCE of 6.90%, which is better than two binary devices. This work demonstrates an effective strategy of utilizing a narrow bandgap donor polymer as the second donor to improve the performance of all-polymer solar cells.

Introduction

Tremendous efforts have been devoted in solution-processed polymer solar cells (PSCs) in the past decades because of their advantages of low-cost, light-weight, flexibility and large-area production.[1] It is reported that the record power conversion efficiency (PCE) is up to ~18%.[2,3] High performance PSCs usually employ a bulk heterojunction (BHJ) architecture, where a narrow bandgap polymer donor (PD) is used as a p-type component and a small molecule or polymer acceptor (SMA or PA) is used as the n-type component.[4–6] The combination of PD and PA (all-PSC) exhibits excellent film processing properties, and superior thermal and mechanical stability, which are essential for practical applications.[7,8] However, the reported highest PCE of all-PSCs is still significantly lower than that of PSCs using SMAs.[9] One reason is the absence of high-efficiency narrow bandgap PAs that could utilize the photons effectively in the near-IR region (700–1000 nm), which has been successfully achieved in SMA PSCs.[10–13] Currently, poly{[*N*,*N*′-bis(2-octyldodecyl)naphthalene-1,4,5,8-bis(dicarboximide)-2,6-diyl]-*alt*-5,5′-(2,2′-bithiophene)} (N2200) is still one of the best PAs due to its high electron mobility, narrow bandgap and excellent compatibility with varieties of PAs.[14–21] Though N2200 thin film displays a relatively wide absorption range of 300–900 nm, the absorption coefficient is dramatically smaller than those high-performance narrow bandgap SMAs in the near-IR region, such as ITIC[10] and Y6.[11] Since the typical high-performance PDs have relatively wider bandgap than N2200,[22] the weak light absorption of N2200 would lead to low EQEs in the near-IR region in comparison to UV-vis region. How to utilize photons in the near-IR region efficiently remains a challenge for all-PSCs. Either developing new narrow bandgap polymers[23–28] or device fabrication technics[29] are needed in future.

In this manuscript, we demonstrate a ternary all-PSC strategy to improving the PCEs by enhancing the absorption in the near-IR region with the loading of second donor. As shown in Scheme 1, three polymers (namely PF2, PM2 and N2200) are studied in the devices. It is worth noting that the chemical structures of PF2 and PM2 have a same benzodithiophene (BDT) building block. PF2 is a relatively wide bandgap polymer in comparison with N2200, which is similar to J51.[17] PM2 is a relatively narrow bandgap polymer which displayed low energy loss in PSCs with SMAs.[30] We first fabricated binary all-

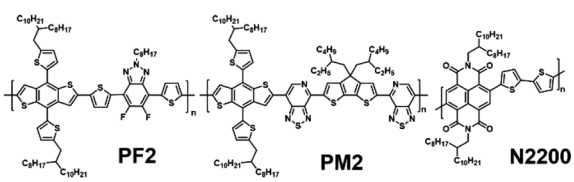

Scheme 1 Chemical structures of PF2, PM2 and N2200.

[a]*Center for Advanced Low-Dimension Materials, State Key Laboratory for Modification of Chemical Fibers and Polymer Materials, College of Materials Science and Engineering, Donghua University, Shanghai 201620, China. E-mail: mwang@dhu.edu.cn; huangj@dhu.edu.cn*

[b]*Institute of Polymer Optoelectronic Materials & Devices, State Key Laboratory of Luminescent Materials and Devices, South China University of Technology, Guangzhou 510640, China. E-mail: dongsheng5175000@126.com*

[c]*Shanghai International College of Design & Innovation, Tongji University, Shanghai 200080, China*

† Electronic supplementary information (ESI) available: Cyclic voltammetry, SCLC mobility, AFM, solar cell device measurements. See DOI: 10.1039/d0ra06143c

PSCs using PF2/N2200 and PM2/N2200 respectively. PF2/N2200 devices exhibited a decent PCE of 6.24% but low EQEs in the range of 600–900 nm. PM2/N2200 displayed better EQEs in the near-IR range but a relatively low PCE of 3.54%. Then PM2 is added into PF2:N2200 blend layer proportionally as the second donor. Finally, the ternary device with a polymer ratio of 1/9/5 (PM2/PF2/N2200) shows an improved PCE of 6.90%, mainly due to the improvement of light absorption in the near-IR range.

Results and discussion

UV-vis absorption

Fig. 1 showed the thin film UV-vis spectra of three polymers. PF2 exhibits an intramolecular charge transfer (ICT) peak at *ca.* 555 nm and a shoulder at *ca.* 605 nm, which indicates the strong intermolecular interaction duo to π–π stacking. The maximum absorption coefficient of PF2 is 9.7×10^4 cm^{-1}. For PM2 thin film, the ICT peak together with the shoulder are around 730 nm and 790 nm, which shows the maximum absorption coefficient of 9.5×10^4 cm^{-1}. It is noted that the narrow bandgap of PM2 is attributed to the strong electron-deficient nature of PT building block.[31–33] For N2200, it is observed that the maximum absorption peak locates at *ca.* 390 nm with an absorption coefficient of 4.3×10^4 cm^{-1}. In the near-IR region, there is an ICT peak together with a shoulder around 700 nm, which gives an absorption coefficient of 3.6×10^4 cm^{-1}. Both peaks' absorption coefficient values of N2200 are dramatically less than those values of PF2 and PM2. In addition, it is clear that PF2 and PM2 show complementary absorption spectra, and PM2 could absorb more photons in the near-IR region than N2200. The complementary absorption feature of above three polymers imply that ternary blend film might be an option to improve the photon absorption from 300 nm to 900 nm than the binary blend films.

Energy levels

The energy levels of donor and acceptor are crucial for PSCs, which should provide the driving force at the D/A interface for holes and electrons separation and transport. We measured their ionization potential and electron affinity by cyclic voltammetry in the thin film state, which approximately represent their HOMO and LUMO to simplify the discussion.[34,35] As shown in Fig. 2, N2200 shows the deepest HOMO (−5.48 eV) and LUMO (−3.88 eV) among three polymers, which allows the charge separation in the PM2/N2200 and PF2/N2200 interface. For PF2 and PM2 polymers, the HOMO of PM2 is −5.34 eV, which is slightly deeper than that of PF2 (−5.25 eV); the LUMO of PM2 is −3.83 eV, which is significantly deeper than that of PF2 (−3.30 eV). This phenomenon implies that the electrons of PF2 could transport to N2200 directly or through PM2, and the holes of N2200 could transport to PF2 directly or through PM2. Overall, PF2–PM2–N2200 system forms an energy cascade model of in the blend film that allows both charge separation and transport properly in PSCs.[36–39]

Solar cell device fabrication

Since both complementary absorption and energy cascade suggest that ternary solar cells is a possible strategy based on these three polymers, we then fabricated all-polymer solar cells to examine the idea with a conventional configuration of ITO/PEDOT:PSS/active layer/PFN-Br/Ag (PEDOT:PSS, poly(3,4-ethylenedioxythiophene) polystyrene sulfonate; PFN-Br, poly(9,9-bis(3′-(*N*,*N*-dimethyl)-*N*-ethylammonium-propyl-2,7-fluorene)-*alt*-2,7-(9,9-dioctylfluorene)) dibromide).[40] The optimal active layer thickness is about 100 nm.

The binary device of PF2:N2200 was firstly fabricated. The optimized condition is under the D : A ratio of 10 : 5 using chlorobenzene (CB) as the solvent with 1,8-diiodooctane additive (DIO, 1% volume). As a result, the best PF2:N2200 device achieved a J_{sc} of 11.85 mA cm^{-2}, a V_{oc} of 0.83 V, an FF of 0.64, and finally give the best PCE of 6.24%. For PM2:N2200 devices, the best PCE is 3.54% under the similar processing condition with a J_{sc} of 9.22 mA cm^{-2}, a V_{oc} of 0.85 V, an FF of 0.45. Fig. 3b provided their EQE curves. One can clearly see the EQE values in the UV-visible light region (300–625 nm) of PF2:N2200 device is substantially greater than those of PM2:N2200 device. But in the near-IR region (>625 nm), the PM2:N2200 device is better. Especially for the region of 800–900 nm, most of electrons are contributed by the absorbance of PM2 since the absorbance of PF2 is very weak here. These difference in the EQE is almost represented in their blend absorption spectra, as shown in Fig. 3c. In addition, it is also noted that PM2:N2200 exhibited a low energy loss of 0.53 eV (E_{loss}, defined as $E_{loss} = E_g^{opt} - eV_{oc}$, where E_g^{opt} is refer to the optical bandgap of blend film).[41,42] The

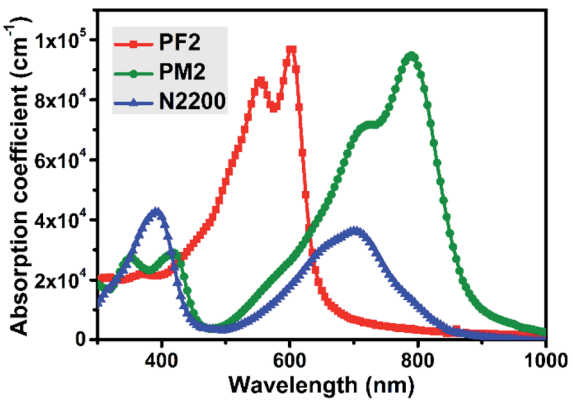

Fig. 1 Film absorption of PF2, PM2 and N2200.

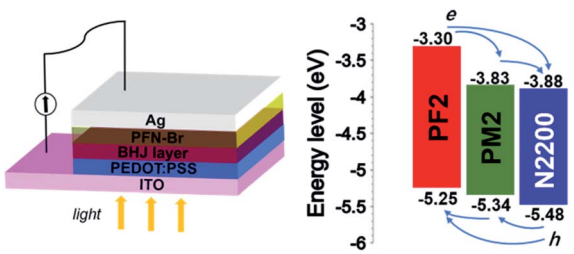

Fig. 2 Solar cell device configuration and energy levels of PF2, PM2 and N2200.

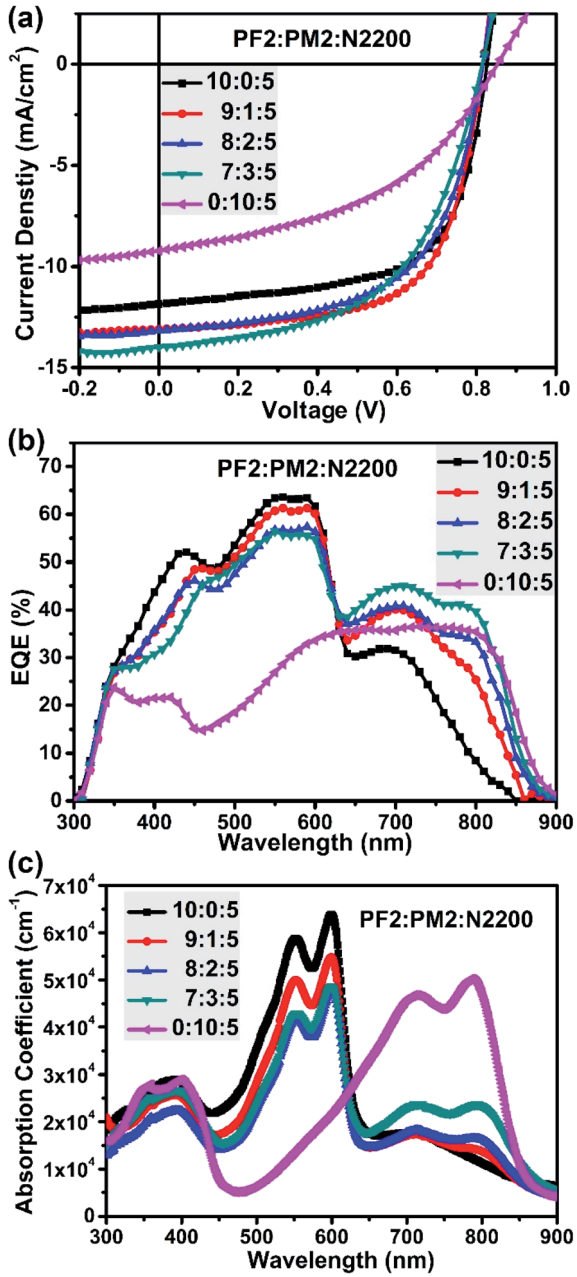

Fig. 3 (a) Device J–V curves; (b) device EQE curves; (c) blend film absorption with different polymer ratios.

low E_{loss} feature of PM2 devices imply that PM2 would be a suitable narrow bandgap donor in the ternary system, which contribute J_{sc} without decreasing V_{oc}.

Since the PF2:N2200 device showed a better PCE than PM2:N2200 device, we then fabricated ternary devices by directly adding PM2 proportionally into the optimal PF2:N2200 blend film to systematically evaluate the influence of PM2 in the ternary system, such as the strong absorption coefficient in the near-IR region and low energy loss. The total D/A ratio is kept as 10 : 5 and CB/DIO (DIO, 1%) mixed-solvent system is used. As shown in Table 1, a significantly improved PCE of 6.90% is achieved for PF2 : PM2 : N2200-based ternary devices at the

Table 1 Solar cell performance of PF2/PM2/N2200 devices

Ratio	J_{sc}[a] (mA cm^{-2})	V_{oc} (V)	FF	PCE[b] (%)
10 : 0 : 5	11.85 (11.17)	0.83	0.64	6.24 (6.18)
9 : 1 : 5	13.10 (12.27)	0.82	0.65	6.90 (6.71)
8 : 2 : 5	13.18 (12.47)	0.82	0.59	6.37 (6.34)
7 : 3 : 5	13.99 (13.06)	0.82	0.55	6.23 (6.20)
0 : 10 : 5	9.22 (9.06)	0.85	0.45	3.54 (3.39)

[a] Numbers in parentheses are J_{sc} calculated from the EQE. [b] Numbers in parentheses are the average PCEs.

ratio of 9 : 1 : 5, which gives a V_{oc} of 0.82 V, a J_{sc} of 13.10 mA cm^{-2} and the same FF of 0.65. The improvement of PCE is attributed to the enhancement of the J_{sc}. When increasing the PM2 weight fraction at the polymer ratio of 8 : 2 : 5, the J_{sc} is 13.18 mA cm^{-2} and V_{oc} is 0.82 V, which are almost identical as the ratio of 9 : 1 : 5. However, the FF decreases to 0.59, and finally results a PCE of 6.37%. When further increasing the PM2 weight fraction at the polymer ratio of 7 : 3 : 5, the J_{sc} improves to 13.99 mA cm^{-2}, the V_{oc} keeps the same and the FF decreases to 0.55. Overall, the PCE drops to 6.23%. In addition, it is interesting that all ternary devices achieved a similar V_{oc} of 0.83 V, which is independent with the weight fraction of PM2 and almost identical to value of PF2:N2200 binary device. This phenomenon implies that the ternary devices form a cascade model and the V_{oc} is up to offset between N2200 and the donor with upper HOMO level. Though we designed two donor polymers with the same BDT building blocks, the polymer alloy was not formed according to the V_{oc} values of ternary devices.[39]

Fig. 3b provide the EQE curves of ternary devices. It is clear that these EQE curves could be divided into two regions. In the UV-visible light region (300–625 nm), the EQE values decreased gradually when increasing the fraction of PM2, which is reasonable since the main UV-vis absorber fraction (PF2) is decreased. In the near-IR region (625–900 nm), the EQE values increased gradually when increasing the weight fraction of PM2. The overall effect shows that the J_{sc} is improved when adding PM2 as the second donor. As shown in Fig. 3c, similar trend could be found in their blend film absorption spectra. However, the FF of ternary devices were also suffered when PM2 fraction is more than 10% in total donor component. Finally, the balanced ratio is achieved at the polymer ratio of 9 : 1 : 5.

To have a deep insight of the exciton generation and dissociation processes, photocurrent density (J_{ph}) *versus* effective voltage (V_{eff}) curves of the five devices were investigated. Fig. 4 provides the J_{ph}–V_{eff} curves of five devices. Here, J_{ph} is defined as $J_{ph} = J_L - J_D$, where J_L and J_D are the current density under AM1.5G light illumination and in dark, respectively. V_{eff} is defined as $V_{eff} = V_0 - V_a$, where V_0 corresponds to the voltage when J_{ph} is equal to zero, and V_a is the applied voltage. It is assumed that all photogenerated excitons could be dissociated into free charges and then collected by two electrodes at high V_{eff}.[36] Therefore, the saturated current density (J_{sat}) is dominated by the maximum exciton generation rate (G_{max}) and follows the equation of $J_{sat} = qLG_{max}$, where q is elementary charge and L is the active layer thickness. For PF2:N2200 device,

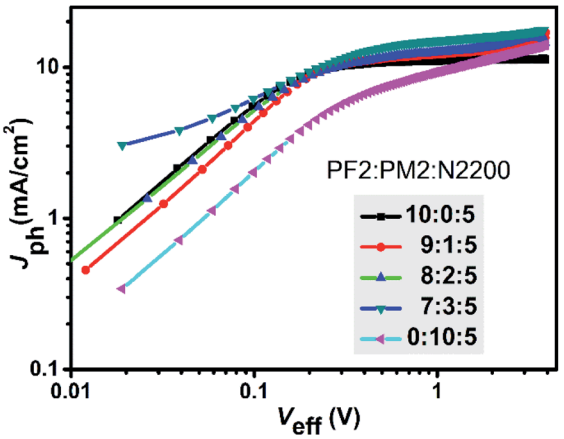

Fig. 4 Photocurrent density (J_{ph}) *versus* effective voltage (V_{eff}) characteristics.

the G_{max} value was 6.78×10^{27} m^{-3} s^{-1} that was calculated at $V_{eff} = 2.0$ V. For ternary devices, their G_{max} values were calculated at the similar V_{eff} and were 7.75×10^{27} m^{-3} s^{-1} (9 : 1 : 5), 7.44×10^{27} m^{-3} s^{-1} (8 : 2 : 5), 8.70×10^{27} m^{-3} s^{-1} (7 : 3 : 5), respectively. For PM2:N2200 device, G_{max} was not obtained as the current density was not saturated. It is clear that the exciton generation rates of ternary devices are faster than PF2:N2200 device. Meanwhile, the charge collection efficiency could be evaluated by J_{ph}/J_{sat} value at the maximal power output condition. For PF2:N2200 device, J_{ph}/J_{sat} was 98.1%, which was higher than that of ternary devices (92.5% at the ratio of 9 : 1 : 5, 91.4% at the ratio of 8 : 2 : 5 and 89.9% at the ratio of 7 : 3 : 5). The result shows that the charge collections in ternary devices are worse than that in PF2:N2200 devices, indicating a negative effect of PM2 loading. In conclusion, the ternary devices have better exciton generation efficiency but exhibit lower charge collection efficiencies and more bimolecular recombination than PF2:N2200 device.

SCLC mobility measurements

Previous studies have revealed that the charge carrier mobility is highly correlated with FF.[43,44] To investigate the FF variations in above ternary devices, we measured the hole mobility of five devices by space-charge-limited current (SCLC) method.[45,46] The hole-only diodes were fabricated with the device structure of ITO/PEDOT:PSS/active layer/MoO_3/Ag, and the *J*–*V* curves are shown in Fig. 5. It is obvious that the hole mobilities are gradually decreased during the increasing of PM2 ratio in the blend, which shows a similar trend of the FF values. For 10 : 0 : 5 and 9 : 1 : 5 blend films, their hole mobilities are on the order of 10^{-4} cm^2 V^{-1} s^{-1} and the PSC devices show a high FF around 0.65. For 8 : 2 : 5 and 7 : 3 : 5 blend films, their hole mobilities decrease to the order of 10^{-5} cm^2 V^{-1} s^{-1} and the PSC devices give decent FF values of 0.55–0.59. The 0 : 10 : 5 film has the lowest hole mobility at the order of 10^{-6} cm^2 V^{-1} s^{-1} and the device displays the lowest FF of 0.45. These results suggest that the hole transport in PM2 phase is undesirable since the mobility decreasing as the function of PM2 ratio. Therefore, FF shows a similar trend as the charge carrier mobility significantly bias the charge recombination. In conclusion, the amount of PM2 should be restricted in the ternary devices to attain a trade-off between J_{sc} and FF.

Light intensity measurements

To reveal the insight of charge recombination dynamics in above PSC devices, we investigated the variations of J_{sc} as function of light intensity. It is reported that the light intensity (L) of J_{sc} in PSCs could be described as the following power relation of $J_{sc} \propto L^a$.[47,48] The deviation from $a = 1$ is typically attributed to the bimolecular recombination. When a approaches to 0.75, space charge effect must be considered. As shown in Fig. 6, all devices show clearly sub-linear dependence of J_{sc} on light intensity. For PM2:N2200 binary device (0 : 10 : 5), it suggests that both bimolecular recombination and the space charge effects contribute to a relatively low a of 0.86. It could be attributed to the low hole mobility of PM2 in the PM2:N2200 blend film, which is in agreement with the hole mobility measurement. For other four devices, there is bimolecular recombination but not significant since their a close to 1. Over all, it suggests that the fraction of PM2 could not be high in the blend films, as the hole transport is not desired in the PM2 phase that promote bimolecular recombination in blend films.

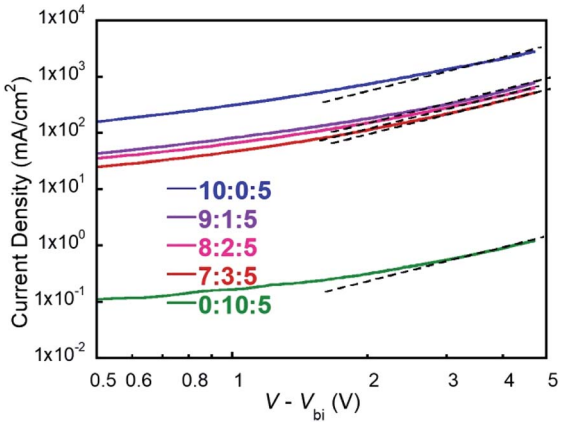

Fig. 5 *J*–*V* curves of devices with different polymer ratios.

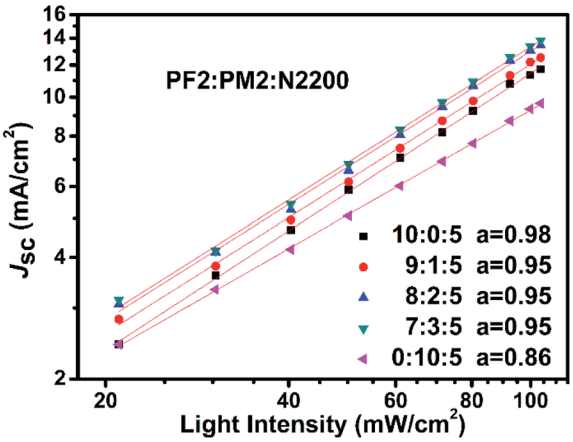

Fig. 6 J_{sc}–*L* curves of devices with different polymer ratios.

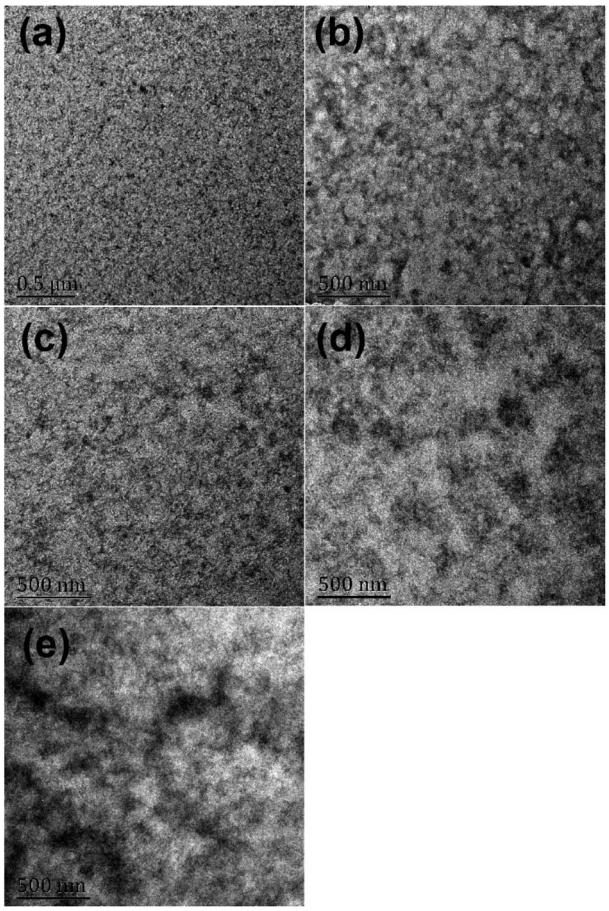

Fig. 7 TEM images of blend films with different polymer (PF2 : PM2 : N2200) ratios: (a) 10 : 0 : 5; (b) 9 : 1 : 5; (c) 8 : 2 : 5; (d) 7 : 3 : 5; (e) 0 : 10 : 5.

Morphology study

To investigate morphology changes when PM2 was loaded into the PF2:N2200 blend film, we prepared these films under the same condition in fabricating PSCs and then tested their morphologies using transmission electron microscope (TEM) in bright-field mode. Fig. 7 provides all the TEM images. The white regions represent the donor polymer domains that absorb the electron weakly, while the dark regions represent the acceptor polymer domains that could prevent the electron transmission. The white-dark contrast and domain size indicate the phase separation scale of donor and acceptor polymers. As shown in Fig. 7a, it is displayed that the donor and acceptor polymers are fine-mixed in PF2:N2200 blend films. One could roughly estimate that both PF2 and N2200 domains' sizes are below 50 nm. For the film of PF2 : PM2 : N2200 = 9 : 1 : 5, as shown in Fig. 7b, it is clearly displayed that the image contrast is enhanced relative to that of Fig. 7a, and the donor-rich domain (white region) size is about ~50–100 nm, which is significantly greater than that in Fig. 7a. In Fig. 7c (PF2 : PM2 : N2200 = 8 : 2 : 5), the phase-separation scale seems similar to that in Fig. 7b. In Fig. 7d (PF2 : PM2 : N2200 = 7 : 3 : 5), the size of donor-rich domain (white region) is over 200 nm, which is substantially greater than that in Fig. 7a–c. Moreover, the size of acceptor-rich domain (dark region) is also enhanced. For PM2:N2200 blend film, as shown in Fig. 7e, the donor-rich domain is formed clearly with the size over 200 nm, which is similar to that in Fig. 7d. In conclusion, the PF2:N2200 blend film shows the best fine-mixed morphology with a preferred size-scale for exciton diffusion. On the contrary, the PM2:N2200 film obtained the worst morphology with a large-scale phase-separation. With small amount PM2 loading (9 : 1 : 5 and 8 : 2 : 5), films could still maintain an acceptable phase-separation scale with interpenetrating polymer network (IPN).

Above results suggest that the loading of PM2 could induce both donor and acceptor polymers forming aggregates and therefore increase the phase-separation scale. It is well-known that the over-sized donor/acceptor domain is difficult for excitons diffusions.[49] In addition, polymer fibre-network is not found in above images.[50] The relatively large-size donor polymer aggregates would also induce grain-boundaries, which increase the energy barriers for charge hoping and prevent the hole transport in different donor domains.[51] Therefore, the hole mobility decreases when the donor domain size increasing. Since both exciton diffusion and hole mobility are crucial for FF, the FF display a trend that is consistent with the phase-separation variations.

Conclusions

In conclusion, we successfully fabricated ternary all-polymer solar cells consisting of two donor polymers with complementary absorption. The second donor PM2 improves the light harvesting due to its strong absorption in the near-IR range, but it also decreases the hole mobility in the blend film and results low FFs when increasing the PM2 ratio. By carefully tuning the ratio of two donor polymers, the trade-off has been achieved at the ratio of 9 : 1 : 5 (PF2 : PM2 : N2200) showing a PCE of 6.90%, which is better than that of two binary devices. More importantly, ternary devices with introducing of PM2 remain a similar V_{oc} in comparing with the PF2:N2200 devices, meaning that there is no extra expense of V_{oc} when increasing the light harvesting in the near-IR region. This work successfully demonstrates a strategy that utilizing a narrow bandgap donor polymer as the second donor to improve the performance of all-polymer solar cells.

Conflicts of interest

There are no conflicts to declare.

Acknowledgements

This work was financially supported by the National Natural Science Foundation of China (21805032), the Pearl River Nova Program of Guangzhou (201906010074) and the Shanghai Design Science (Category IV) Peak Discipline Open Grant (DB8109).

References

1 L. Lucera, F. Machui, P. Kubis, H. D. Schmidt, J. Adams, S. Strohm, T. Ahmad, K. Forberich, H.-J. Egelhaaf and C. J. Brabec, *Energy Environ. Sci.*, 2016, **9**, 89–94.
2 Q. Liu, Y. Jiang, K. Jin, J. Qin, J. Xu, W. Li, J. Xiong, J. Liu, Z. Xiao, K. Sun, S. Yang, X. Zhang and L. Ding, *Sci. Bull.*, 2020, **65**, 272–275.
3 L. Meng, Y. Zhang, X. Wan, C. Li, X. Zhang, Y. Wang, X. Ke, Z. Xiao, L. Ding, R. Xia, H.-L. Yip, Y. Cao and Y. Chen, *Science*, 2018, **361**, 1094–1098.
4 G. Yu, J. Gao, J. C. Hummelen, F. Wudl and A. J. Heeger, *Science*, 1995, **270**, 1789–1791.
5 C. Zhao, J. Wang, J. Jiao, L. Huang and J. Tang, *J. Mater. Chem. C*, 2019, **8**, 28–43.
6 Q. Yue, W. Liu and X. Zhu, *J. Am. Chem. Soc.*, 2020, **142**, 11613–11628.
7 H. Kang, W. Lee, J. Oh, T. Kim, C. Lee and B. J. Kim, *Acc. Chem. Res.*, 2016, **49**, 2424–2434.
8 C. Lee, S. Lee, G.-U. Kim, W. Lee and B. J. Kim, *Chem. Rev.*, 2019, **119**, 8028–8086.
9 T. Jia, J. Zhang, W. Zhong, Y. Liang, K. Zhang, S. Dong, L. Ying, F. Liu, X. Wang, F. Huang and Y. Cao, *Nano Energy*, 2020, **72**, 104718.
10 Y. Lin, J. Wang, Z.-G. Zhang, H. Bai, Y. Li, D. Zhu and X. Zhan, *Adv. Mater.*, 2015, **27**, 1170–1174.
11 J. Yuan, Y. Zhang, L. Zhou, G. Zhang, H.-L. Yip, T.-K. Lau, X. Lu, C. Zhu, H. Peng, P. A. Johnson, M. Leclerc, Y. Cao, J. Ulanski, Y. Li and Y. Zou, *Joule*, 2019, **3**, 1140–1151.
12 H. Yao, Y. Chen, Y. Qin, R. Yu, Y. Cui, B. Yang, S. Li, K. Zhang and J. Hou, *Adv. Mater.*, 2016, **28**, 8283–8287.
13 F. Liu, Z. Zhou, C. Zhang, J. Zhang, Q. Hu, T. Vergote, F. Liu, T. P. Russell and X. Zhu, *Adv. Mater.*, 2017, **29**, 1606574.
14 H. Yan, Z. Chen, Y. Zheng, C. Newman, J. R. Quinn, F. Dötz, M. Kastler and A. Facchetti, *Nature*, 2009, **457**, 679–686.
15 Z. Li, L. Ying, P. Zhu, W. Zhong, N. Li, F. Liu, F. Huang and Y. Cao, *Energy Environ. Sci.*, 2019, **12**, 157–163.
16 B. Fan, W. Zhong, L. Ying, D. Zhang, M. Li, Y. Lin, R. Xia, F. Liu, H.-L. Yip, N. Li, Y. Ma, C. J. Brabec, F. Huang and Y. Cao, *Nat. Commun.*, 2019, **10**, 4100.
17 L. Gao, Z.-G. Zhang, L. Xue, J. Min, J. Zhang, Z. Wei and Y. Li, *Adv. Mater.*, 2016, **28**, 1884–1890.
18 Z. Li, X. Xu, W. Zhang, X. Meng, W. Ma, A. Yartsev, O. Inganäs, M. R. Andersson, R. A. J. Janssen and E. Wang, *J. Am. Chem. Soc.*, 2016, **138**, 10935–10944.
19 Z. Li, X. Xu, W. Zhang, X. Meng, Z. Genene, W. Ma, W. Mammo, A. Yartsev, M. R. Andersson, R. A. J. Janssen and E. Wang, *Energy Environ. Sci.*, 2017, **10**, 2212–2221.
20 X. Liu, C. Zhang, C. Duan, M. Li, Z. Hu, J. Wang, F. Liu, N. Li, C. J. Brabec, R. A. J. Janssen, G. C. Bazan, F. Huang and Y. Cao, *J. Am. Chem. Soc.*, 2018, **140**, 8934–8943.
21 L. Zhu, W. Zhong, C. Qiu, B. Lyu, Z. Zhou, M. Zhang, J. Song, J. Xu, J. Wang, J. Ali, W. Feng, Z. Shi, X. Gu, L. Ying, Y. Zhang and F. Liu, *Adv. Mater.*, 2019, **31**, 1902899.
22 P. Zhu, B. Fan, L. Ying, F. Huang and Y. Cao, *Chem.–Asian J.*, 2019, **14**, 3109–3118.
23 C. Dou, J. Liu and L. Wang, *Sci. China: Chem.*, 2017, **60**, 450–459.
24 K. Feng, J. Huang, X. Zhang, Z. Wu, S. Shi, L. Thomsen, Y. Tian, H. Y. Woo, C. R. McNeill and X. Guo, *Adv. Mater.*, 2020, 2001476.
25 Z.-G. Zhang, Y. Yang, J. Yao, L. Xue, S. Chen, X. Li, W. Morrison, C. Yang and Y. Li, *Angew. Chem., Int. Ed.*, 2017, **56**, 13503–13507.
26 H. Yao, F. Bai, H. Hu, L. Arunagiri, J. Zhang, Y. Chen, H. Yu, S. Chen, T. Liu, J. Y. L. Lai, Y. Zou, H. Ade and H. Yan, *ACS Energy Lett.*, 2019, **4**, 417–422.
27 G. Feng, J. Li, F. J. M. Colberts, M. Li, J. Zhang, F. Yang, Y. Jin, F. Zhang, R. A. J. Janssen, C. Li and W. Li, *J. Am. Chem. Soc.*, 2017, **139**, 18647–18656.
28 S. Liu, Y. Firdaus, S. Thomas, Z. Kan, F. Cruciani, S. Lopatin, J.-L. Brédas and P. M. Beaujuge, *Angew. Chem., Int. Ed.*, 2018, **57**, 531–535.
29 Y. Xu, J. Yuan, S. Liang, J.-D. Chen, Y. Xia, B. W. Larson, Y. Wang, G. M. Su, Y. Zhang, C. Cui, M. Wang, H. Zhao and W. Ma, *ACS Energy Lett.*, 2019, **4**, 2277–2286.
30 M. Wang, H. Wang, M. Ford, J. Yuan, C.-K. Mai, S. Fronk and G. C. Bazan, *J. Mater. Chem. A*, 2016, **4**, 15232–15239.
31 N. Blouin, A. Michaud, D. Gendron, S. Wakim, E. Blair, R. Neagu-Plesu, M. Belletête, G. Durocher, Y. Tao and M. Leclerc, *J. Am. Chem. Soc.*, 2008, **130**, 732–742.
32 L. Ying, B. B. Y. Hsu, H. Zhan, G. C. Welch, P. Zalar, L. A. Perez, E. J. Kramer, T.-Q. Nguyen, A. J. Heeger, W.-Y. Wong and G. C. Bazan, *J. Am. Chem. Soc.*, 2011, **133**, 18538–18541.
33 H. Zhou, L. Yang and W. You, *Macromolecules*, 2012, **45**, 607–632.
34 C. M. Cardona, W. Li, A. E. Kaifer, D. Stockdale and G. C. Bazan, *Adv. Mater.*, 2011, **23**, 2367.
35 J.-L. Bredas, *Mater. Horiz.*, 2013, **1**, 17–19.
36 L. Lu, T. Xu, W. Chen, E. S. Landry and L. Yu, *Nat. Photonics*, 2014, **8**, 716–722.
37 Y. Yang, W. Chen, L. Dou, W.-H. Chang, H.-S. Duan, B. Bob, G. Li and Y. Yang, *Nat. Photonics*, 2015, **9**, 190–198.
38 P. P. Khlyabich, B. Burkhart and B. C. Thompson, *J. Am. Chem. Soc.*, 2012, **134**, 9074–9077.
39 Z. Wang, X. Zhu, J. Zhang, K. Lu, J. Fang, Y. Zhang, Z. Wang, L. Zhu, W. Ma, Z. Shuai and Z. Wei, *J. Am. Chem. Soc.*, 2018, **140**, 1549–1556.
40 T. Yang, M. Wang, C. Duan, X. Hu, L. Huang, J. Peng, F. Huang and X. Gong, *Energy Environ. Sci.*, 2012, **5**, 8208–8214.
41 M. Wang, H. Wang, T. Yokoyama, X. Liu, Y. Huang, Y. Zhang, T.-Q. Nguyen, S. Aramaki and G. C. Bazan, *J. Am. Chem. Soc.*, 2014, **136**, 12576–12579.
42 W. Li, K. H. Hendriks, A. Furlan, M. M. Wienk and R. A. J. Janssen, *J. Am. Chem. Soc.*, 2015, **137**, 2231–2234.
43 C. M. Proctor, J. A. Love and T.-Q. Nguyen, *Adv. Mater.*, 2014, **26**, 5957–5961.
44 J. A. Bartelt, D. Lam, T. M. Burke, S. M. Sweetnam and M. D. McGehee, *Adv. Energy Mater.*, 2015, **5**, 1500577.
45 A. Rose, *Phys. Rev.*, 1955, **97**, 1538–1544.

46 M. A. Lampert and P. Mark, *Current Injection in Solids*, Academic, New York, 1970.
47 C. M. Proctor, C. Kim, D. Neher and T.-Q. Nguyen, *Adv. Funct. Mater.*, 2013, **23**, 3584–3594.
48 A. K. K. Kyaw, D. H. Wang, V. Gupta, W. L. Leong, L. Ke, G. C. Bazan and A. J. Heeger, *ACS Nano*, 2013, **7**, 4569–4577.
49 M. Menke and R. J. Holmes, *Energy Environ. Sci.*, 2014, **7**, 499–512.
50 J. J. van Franeker, G. H. L. Heintges, C. Schaefer, G. Portale, W. Li, M. M. Wienk, P. van der Schoot and R. A. J. Janssen, *J. Am. Chem. Soc.*, 2015, **137**, 11783–11794.
51 R. Noriega, J. Rivnay, K. Vandewal, F. P. V. Koch, N. Stingelin, P. Smith, M. F. Toney and A. Salleo, *Nat. Mater.*, 2013, **12**, 1038–1044.